Interpreting a period-adding bifurcation scenario in neural bursting patterns using border-collision bifurcation in a discontinuous map of a slow control variable*

Mo Juan(莫 娟)[a], Li Yu-Ye(李玉叶)[a], Wei Chun-Ling(魏春玲)[a], Yang Ming-Hao(杨明浩)[a], Gu Hua-Guang(古华光)[a]†, Qu Shi-Xian(屈世显)[b], and Ren Wei(任 维)[a]

[a] College of Life Science, Shaanxi Normal University, Xi'an 710062, China
[b] College of Physics and Information Technology, Shaanxi Normal University, Xi'an 710062, China

(Received 30 December 2009; revised manuscript received 24 January 2010)

To further identify the dynamics of the period-adding bifurcation scenarios observed in both biological experiment and simulations with the differential Chay model, this paper fits a discontinuous map of a slow control variable of the Chay model based on simulation results. The procedure of period adding bifurcation scenario from period k to period $k+1$ bursting (k = 1, 2, 3, 4) involved in the period-adding cascades and the stochastic effect of noise near each bifurcation point is also reproduced in the discontinuous map. Moreover, dynamics of the border-collision bifurcation are identified in the discontinuous map, which is employed to understand the experimentally observed period increment sequence. The simple discontinuous map is of practical importance in the modeling of collective behaviours of neural populations like synchronization in large neural circuits.

Keywords: period-adding bifurcation, border-collision bifurcation, discontinuous maps, neural bursting pattern

PACC: 0547, 8728, 8730

1. Introduction

Oscillation is a typical characteristic of many nonlinear systems. Various nonlinear oscillations emerge in chemical, engineering, and biological systems.[1−4] In biological systems, bursting oscillation with diverse temporal patterns in neuronal firing activities has been shown to play critical roles in almost all important cognitive functions including sensory coding, memory formation, perception, and decision making.[3,4] Therefore, elucidation of the dynamics of neuronal bursting patterns and the bifurcation mechanisms of bursting pattern transitions is essential for understanding the information processing in the brain. In the past twenty years, great progress in nonlinear dynamics has inspired an increasing enthusiasm in the study on nonlinear bursting in neuronal firing activities.[2−33] Such an enthusiastic study not only sheds light on neuroscientists' comprehension of neuronal firing behaviours but also enriches nonlinear scientists' knowledge of nonlinear phenomena in the natural world.

In studies on the dynamics of bursting patterns, a series of differential equation models have been formulated,[5−17] including the ionic conductance based model such as Chay model[5−7] and empirical ones such as the Hindmarsh–Rose (HR) model.[9−13] Both Chay and HR models are the three-variable ones capturing essential features of bursting neurons. These models manifest common dynamical mechanisms for bursting neurons, although the ionic basis involved may be different. In general, these models illustrate the generation of firing spikes by a fast subsystem and represent modulation of the mode of the spike train by a slow subsystem,[2,14,15,17,32] respectively. In Chay model intracellular calcium concentration controls the beginning and termination of a burst through a calcium-dependent potassium mechanism.[5−7,32] The fast and slow subsystems can be identified by separating their timescales.[2,14,15,17,32] The bifurcation mechanisms of the fast subsystem can be revealed by using the slow

*Project supported by the National Natural Science Foundation of China (Grant Nos. 10774088, 10772101, 30770701 and 10875076) and the Fundamental Research Funds for the Central Universities (Grant No. GK200902025).
†Corresponding author. E-mail: guhuaguang@263.net
© 2010 Chinese Physical Society and IOP Publishing Ltd

variable as a bifurcation parameter. With this approach a class of spiking, bursting and transition from spiking to bursting have been explained in terms of the bifurcation theory.[2,32,34,35] Important statistics such as the number of spikes and duration of inter-spike intervals in a burst have been found to be related to the distance from the critical transition between spiking and bursting, quantitatively showing the changes of bursting behaviour.[34]

In studies on the bifurcation cascades underpinning bursting pattern transitions,[5−11,16,17,31] a set of bifurcation scenarios (cascade bifurcations), including period-doubling, period-adding with chaos, and period-adding without chaos, have been systematically observed in simulation with the neuronal models by adjusting parameters related to the slow variable. Following such theoretical simulations, those bifurcation scenarios were also observed in biological experiments on an experimental pacemaker by manipulating similar biological parameters.[18−28] These fundamental studies of the regularities of bursting pattern transitions are of great practical interest because apprehension of conditions triggering such transitions is critical for understanding the changes of functional brain states.[3,4] In contrast to the impressive progress in studies on the dynamics of the formation of various bursting patterns,[34] explanation for transition between the bursting oscillations in terms of precise bifurcation theory is still relatively superficial.[15,17,29,30]

Among the observed bifurcation scenarios of bursting mode, period-adding bifurcation scenario is of unique practical importance.[5,17,18,20−23,28,31] In this bifurcation scenario the bursting pattern changes directly from period one to period two, to period three, and so on. The neuronal firing pattern is in turn single spike burst, doublet burst, and triplet burst, and so on (see Refs. [18], [20]–[23], [28] and Fig. 1 in Section 2). With such a bifurcation cascade, neurons can use single spike, doublet, and triplet as 'neuronal codes' to represent the variation and magnitude of the parameter. Unfortunately, the bifurcation mechanism underpinning the experimentally observed period-adding bifurcation remains unclear.[17,29]

Reduction of differential equation models to low-dimensional maps is an elucidatory approach to investigate the bifurcation dynamics of the original system of continuous flow.[32] Recently, cascade bifurcation behaviours seen in the differential models of various systems, including mechanical systems involving friction, electrical circuits containing diodes, transistor systems, and earthquake engineering systems, have been studied by reduction of the differential models to the discontinuous map of an appropriate variable.[36−53] The bifurcation of oscillations in the original continuous flow system has been deeply explained by analysing the discontinuous map.

A theoretical method for reducing differential neuronal models to one-dimensional maps was developed in a previous study.[32] Differential models containing a slow and a fast subsystem were changed to the form of a singularly perturbed system, bifurcation dynamics of the fast subsystem driven by the slow variable was then elucidated as entering burst from a Hopf bifurcation and terminating burst from a homoclinic bifurcation in which the limit cycle merges with a saddle and the period of the limit cycle becomes infinite, the fast subsystem reaches a coexisted stable node. The stable node and the saddle merge and disappear via saddle-node bifurcation at a certain parameter value locating between the Hopf bifurcation and the homoclinic bifurcation. By averaging the integration of the slow subsystem along the trajectory of the fast subsystem and qualitatively analysing homoclinic bifurcation of the singularly perturbed system, the differential model was reduced to a one-dimensional map of the slow variable as the bifurcation parameter. This map exhibits unimodal characteristics with a boundary layer corresponding to the homoclinic bifurcation. Studying bifurcation of the constructed map reveals the dynamics underpinning transitions between various spiking and bursting patterns. But unfortunately, this method is complex and difficult.

Alternatively, the map which can also be acquired by fitting the numerical simulation results, was used in previous studies.[12,13] In the present study, the map which was acquired by fitting the numerical simulation results of Chay model, was a discontinuous map composed of a linear left-hand part with a positive slop and a horizontal right-hand part. There is a gap between the two parts.

The rest of this paper is organized as follows. Section 2 presents the experimental methods and results. Section 3 introduces the deterministic and stochastic Chay model and provides results of numeric simulation of the experimentally observed period-adding bifurcation scenario. Section 4 is a description of the discontinuous map of the slow variable (intracellular calcium concentration) of Chay model, resulted from fitting numerical simulation. Section 5 gives the numerical simulation results of the map, the period-adding

bifurcation process in the slow variable iteration series. Section 6 is an analysis of the discontinuous map to show the mechanism of period-adding bifurcation sequence. In Section 7 we applied a generic concept to the constructed map, building a relationship to other kinds of period adding bifurcation scenario in discontinuous map. Section 8 is the discussion and conclusion.

2. Experimental model and results

2.1. Experimental model

For the purpose of a comparative study of bifurcation scenarios in biological experimentation and dynamical investigation, this study employed an experimental neural pacemaker model manifesting very rich bursting behaviours and a generic neuronal model capturing essential dynamics of bursting activities.[18−28] Experimental neural pacemakers were produced by subjecting the sciatic nerve to chronic ligatures using adult male Sprague Dawley rats (200–300 g). Rats were anesthetized with pentobarbital sodium (40 mg/kg, ip). Three or four loose ligatures were made at the level of the middle thigh of the left sciatic nerve. After a survival time of 8–12 days, the animals were re-anesthetized and prepared with tracheal cannula. The previously ligatured site in which the pacemakers were formed was exposed and was perfused continuously with 34 °C Kreb's solution (NaCl 150 mM, KCl 5 mM, $MgCl_2$ 1 mM, $CaCl_2$ 1.2 mM, N-2-hydroxyethylpiperazine-N-ethane-sulphonicacid (HEPES) 5 mM, and PH=7.4). The ligatured site was disconnected from the receptive field by acutely crushing the nerve just peripheral to the injury. About 20–30 mm proximal to the injured site, the sciatic nerve was exposed separately and covered with 34 °C paraffin oil. The spontaneous spike trains of individual fibres ending at the injured site were recorded in this oil pool by desheathing the nerve, separating a fine bundle of fibres which were disconnected from the central nervous system but whose connection to this ligatured site was left intact, and placing this fine bundle on a single platinum electrode (29 μm in diameter) referred to a nearby indifference. The spontaneous spike trains were recorded with a PowerLab system (Australia) with sampling frequency being 10.0 kHz. Meanwhile the spike trains were monitored with the recording system during the whole experiment to make sure that the recording is of a single unit. The time intervals between the maximal values of the successive spikes were recorded seriatim as inter-spike interval (ISI) series. The extra-cellular calcium concentration ($[Ca^{2+}]_o$) was adjusted as the control parameter in experiments.

2.2. Experimental results

A series of bifurcation scenarios of firing patterns generated by the experimental neural pacemaker were discovered, including period-doubling bifurcation cascade,[18−20] period-adding bifurcation with chaos,[18,20,22,28] and period-adding bifurcation without chaos.[21−23,28] In what follows, we particularly study the period-adding bifurcation scenario without chaos.

Figure 1 shows a typical example from 36 cases of such period-adding bifurcation, induced by slowly adjusting extra-cellular calcium concentration ($[Ca^{2+}]_o$) from 1.2 mmol/L to 0 mmol/L. The bursting is period 1 under the control condition wherein $[Ca^{2+}]_o$ is 1.2 mmol/L. During decrease of $[Ca^{2+}]_o$, the bursting pattern evolves from period k to a stochastic alternating between period k and period $k+1$ trajectories, to period $k+1$ ($k = 1, 2, 3, 4$). The overall profile of this bifurcation diagram is a period-adding without chaos in which stochastic 'jumping' between two neighbouring periodic orbits is evoked by internal noise in the vicinity of each bifurcation from period k to period $k+1$.

The firing train of the stochastic bursting lying between period 2 and period 3 trajectories is exemplified in Fig. 1(d). With a period 2 or period 3 burst defined as an event and the interval between two successive events as inter-event interval (IEI), an exponentially decaying multi-peak distribution is clearly seen in IEI histogram of this stochastic bursting pattern (Fig. 2(b)). The first return map of its IEI series exhibits a lattice structure, as shown in Fig. 2(d). Such uncorrelated properties, combined with other analysis in previous studies,[22] demonstrate the stochastic nature of the bursting. This demonstration is valid for the stochastic bursting observed between period k and period $k+1$ ($k = 1, 2, 3, 4$). The stochastic bursting has been related to the phenomenon of stochastic resonance.[21,26,33]

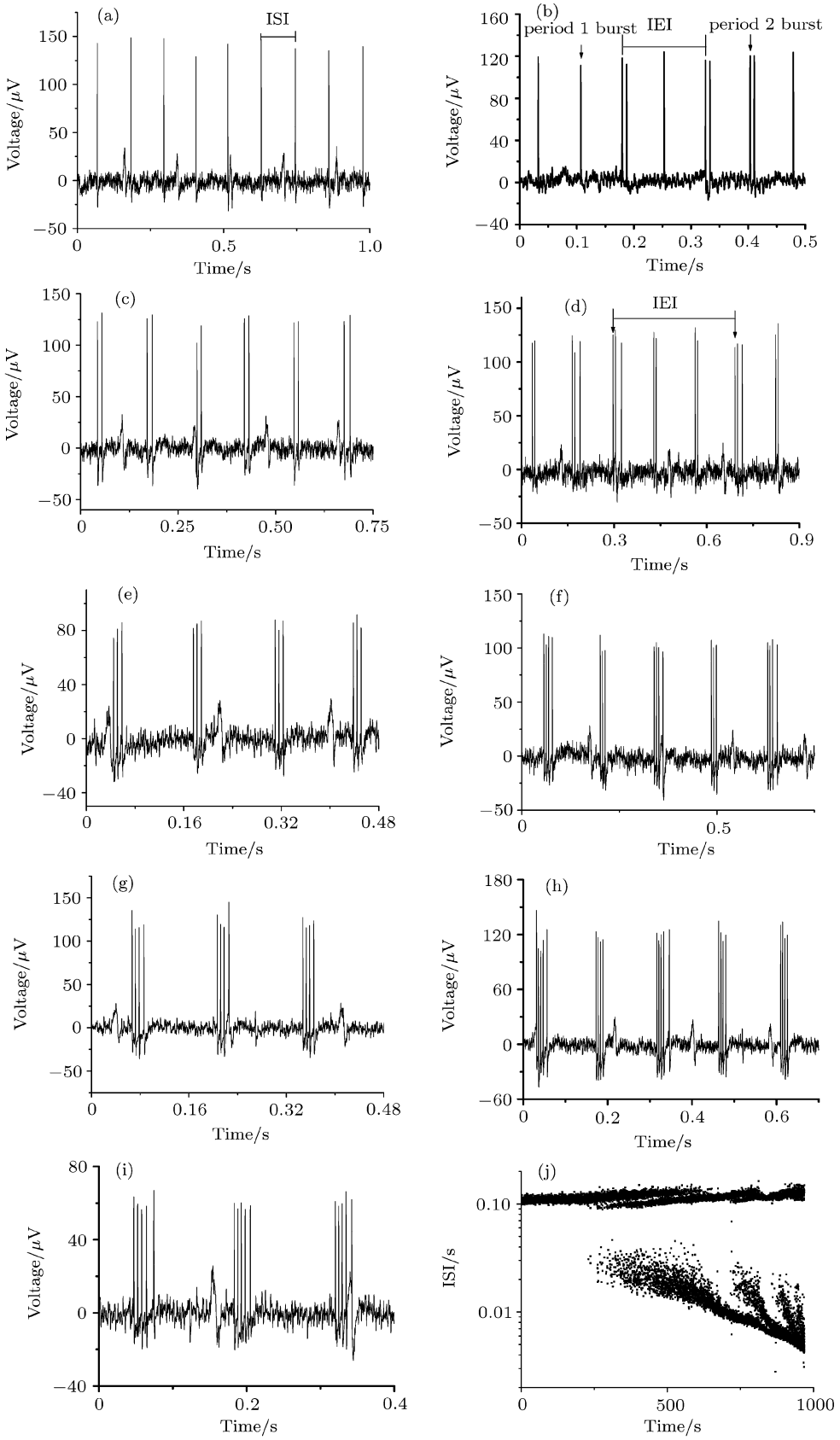


Fig. 1. (a) Firing train of period 1 burstings. (b) Firing train of stochastic burstings lying between period 1 and period 2. (c) Firing train of period-2 burstings. (d) Firing train of stochastic burstings lying between period 2 and period 3. (e) Firing train of period–3 burstings. (f) Firing train of stochastic burstings lying between period 3 and period 4. (g) Firing train of period-4 burstings. (h) Firing train of stochastic burstings lying between period 4 and 5. (i) Firing train of period-5 burstings. (j) The bifurcation scenarios of bursting patterns from period 1 to period 5 with stochastic bursting.

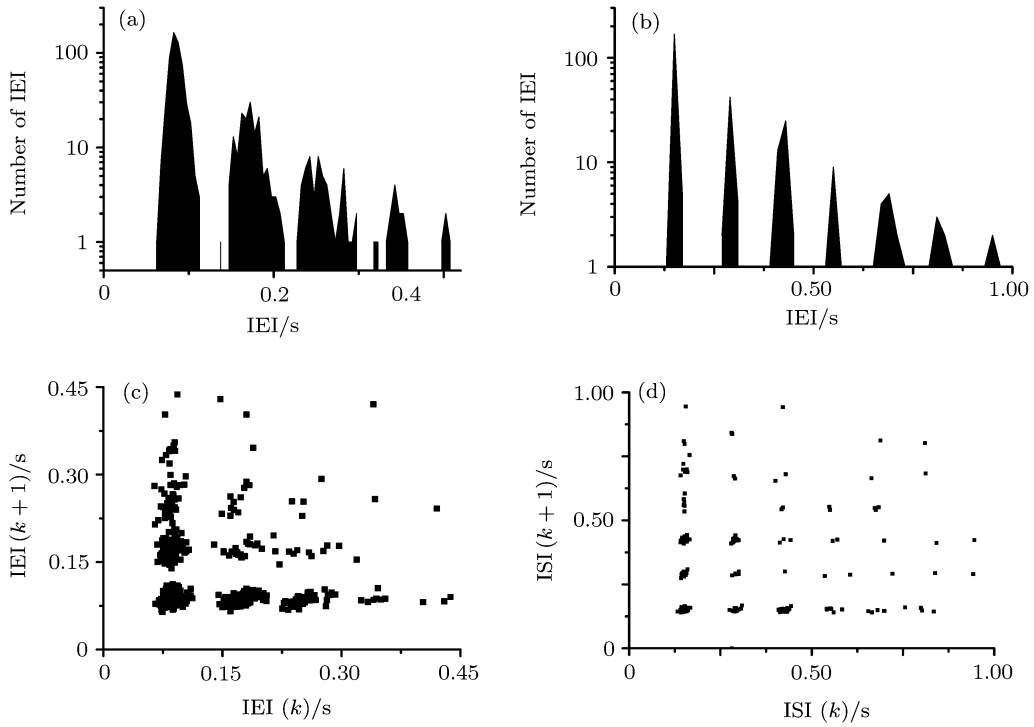


Fig. 2. (a) The IEI histogram of stochastic burstings lying between period-1 and period-2 bursting when period-2 burst is chosen as an event. (b) The IEI histogram of stochastic burstings lying between period-2 and period-3 bursting when period-3 burst is chosen as an event. (c) First return map of IEI series corresponding to (a). (d) First return map of IEI series corresponding to (b).

3. Theoretical model and numerical simulation

3.1. Theoretical Chay model

Chay model[5–7] is a biological conductance based neuronal model verified to be able to reproduce bursting behaviour of several kinds of typical excitable cells including the pancreatic β-cells and the experimental neural pacemaker. Thus, we simulated the above experimental observation with deterministic and stochastic Chay models. The deterministic Chay model is as follows:

$$\frac{\mathrm{d}V}{\mathrm{d}t} = g_i m_\infty^3 h_\infty (v_i - V) + g_{kv}(v_k - V)n^4 + g_{kc}\frac{C}{1+C}(v_k - V) + g_l(v_l - V), \quad (1)$$

$$\frac{\mathrm{d}n}{\mathrm{d}t} = \frac{n_\infty - n}{\tau_n}, \quad (2)$$

$$\frac{\mathrm{d}C}{\mathrm{d}t} = \rho[m_\infty^3 h_\infty (v_c - V) - k_c C], \quad (3)$$

where t is the time (the independent variable). The dependent variables are V (the membrane potential), n (the probability of potassium channel activation) and C (the dimensionless intracellular concentration of calcium ion). In Eq. (2), $\tau_n = 1/(\lambda_n(\alpha_n + \beta_n))$. The explicit interpretation of Chay model was given in Refs. [5]–[7]. In this paper, the parameter values are $v_i = 100$ mV, $v_k = -75$ mV, $v_l = -40$ mV, $g_{kv} = 1700$ mS/cm^2, $g_i = 1800$ mS/cm^2, $g_l = 7$ mS/cm^2, $g_{kc} = 20$ mS/cm^2, $k_c = 3.3/18$, $\rho = 0.27$ mV$^{-1}\cdot$ mS/cm^2 and $\lambda_n = 235$.

The stochastic Chay model is formed by adding a Gaussian white noise term to Eq. (1) to represent fluctuations inevitable in experimentation. The added stochastic factor, $\xi(t)$, possesses statistical properties as $\langle\xi(t)\rangle = 0$ and $\langle\xi(t)\xi(t')\rangle = 2D\delta(t-t')$, where D is the noise density and $\delta(\bullet)$ is the Dirac-δ function.

The v_c is the reversal potential of calcium ion. It is associated with extra-cellular calcium concentration ($[\mathrm{Ca}^{2+}]_\mathrm{o}$) via the Nernst equation and thus was taken as the bifurcation control parameter. The deterministic and stochastic Chay models were solved by the Mannella numeric integrating method[54] with integration time step being 10^{-4} sec. Upstrokes of the voltage reached the amplitude of -25.0 mV were counted as spikes.

3.2. Period-adding bifurcation in the deterministic Chay model

In the deterministic Chay model with $232 < \lambda_n < 245$, the period-adding bifurcation without chaos can be induced by adjusting v_c. Figure 3(a) shows the simulated bifurcation diagram of ISI with $\lambda_n = 235$, v_c is decreased from 150 mV to 32 mV, in which bursting behaviour of the system evolves from period 1 (v_c=150.00–115.18 mV) to period 2 (v_c=115.17–69.03 mV), to period 3 (v_c=69.02–48.94 mV), to period 4 (v_c=48.93–37.60 mV), and to period 5 (v_c=37.59–32.0 mV). At the bifurcations from period k to $k+1$ ($k = 1$, 2, 3, 4), a singular and sudden emerge of a new spike results in a new periodic orbit with one more cycle.

The trajectory and the evolution of V and C of a period-3 bursting pattern under $v_c = 50$ mV are shown in Figs. 3(b) and 3(c), respectively. The C is the slow control variable in Chay model.[5–7] Labeling C values corresponding to peak values of voltage ($V_{\max}$) as C_{Vm} (triangles on upper line in Fig. 3(c)), we obtain a period-adding bifurcation scenario in the Poincaré map of C (in $V = V_{\max}$ plane) with respect to v_c as shown in Fig. 3(d).

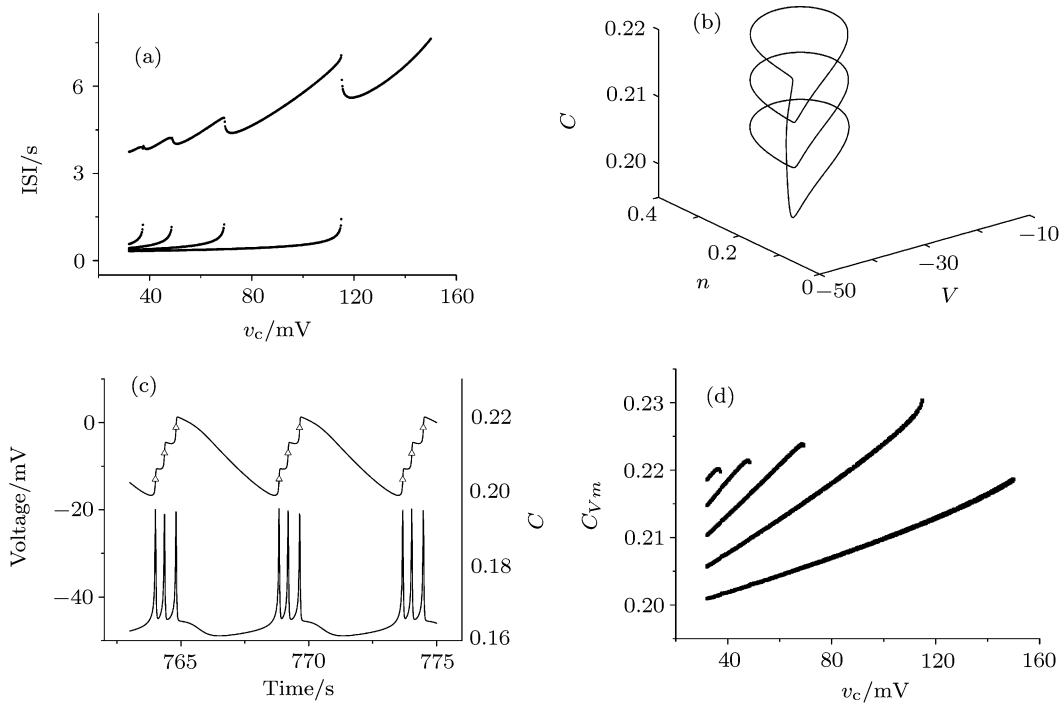


Fig. 3. (a) The bifurcation diagram of ISI with respect to v_c in deterministic Chay model. (b) Trajectory of period-3 bursting in (V, n, C) phase space with $v_c = 50$ mV. (c) The bursting train of V (lower) and C (upper) with $v_c = 50$ mV, the C value corresponding to peak values of V, represented by triple angle, labeled as C_{Vm}. (d) The bifurcation diagram of C_{Vm} with respect to v_c.

3.3. Period-adding bifurcation in stochastic Chay model

With added noise, the simulated period-adding bifurcation scenario of ISI changes to period-adding bifurcation with stochastic bursting, this is very similar to the experimental observation. Calculated the profile similar to simulation with the deterministic Chay model, the stochastic Chay model exhibits stochastic bursting patterns between period k and period $k+1$ bursting ($k = 1$, 2, 3, 4), as shown in Fig. 4(a) in which D=0.0005. Overlaps composed of period k points and period $k+1$ points appear between period k and period $k+1$ orbits. Such a structure of bifurcation diagram can be observed in a large range of noise density. The bursting pattern lying between period k and period $k+1$ ($k = 1$, 2, 3, 4) results from stochastic transitions between period k and period $k+1$ orbits, as shown in Fig. 4(b). Similar to the experimental results, the first return map of IEI series and the IEI histogram of this stochastic bursting also manifest lattice structure and exponentially

decaying multiple peaks, respectively (Figs. 4(c) and 4(d)).

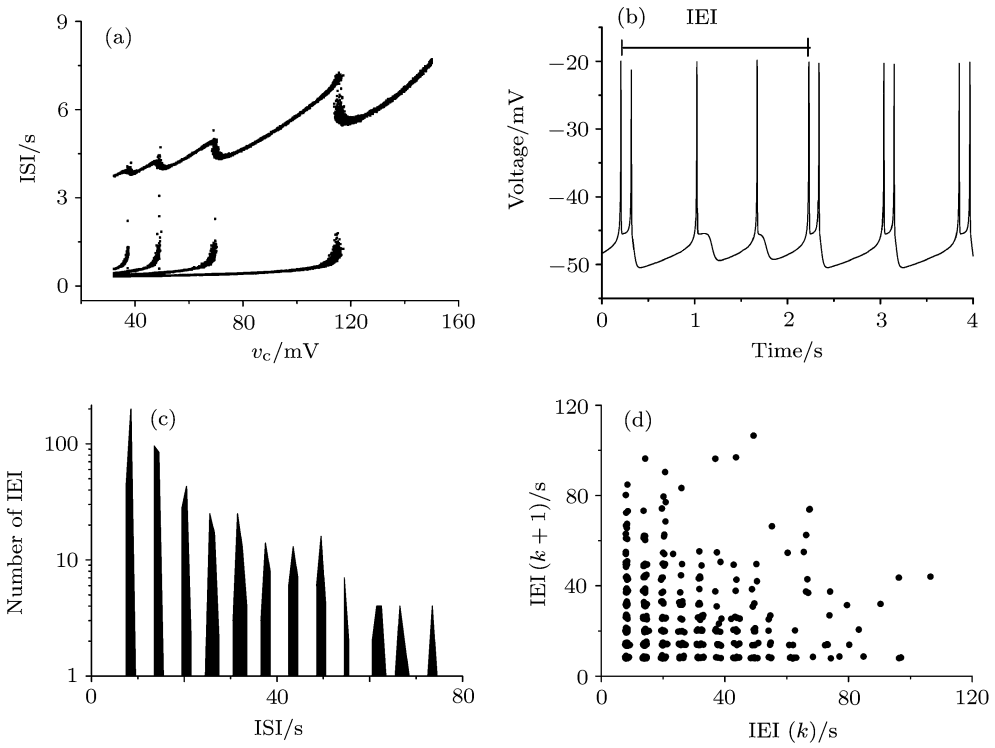
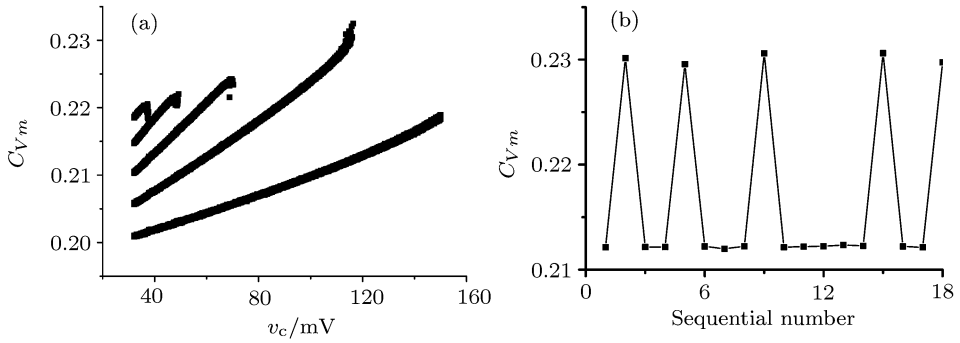


Fig. 4. (a) The bifurcation diagram of ISI with respect to v_c in the stochastic Chay model with noise density D=0.0005. (b) The bursting train of stochastic bursting between period 1 and period 2, a stochastic transition between period-1 burst and period-2 burst (v_c = 115.5 mV and D=0.0005). (c) The IEI histogram of the stochastic bursting (v_c = 115.5 mV and D=0.0005, and period-2 burst is defined as an event). (d) The return map of IEI series in (c).

3.4. Period adding bifurcation of C_{Vm} in stochastic Chay model

The bifurcation of C_{Vm} obtained from simulation with the stochastic Chay model is shown in Fig. 5(a). Different from the deterministic model, it exhibits stochastic iterations between period k and $k+1$ periodic points in the vicinity of each of the bifurcations. For example, the stochastic iteration series between periods 1 and 2 exhibits stochastic transitions between the period-1 point and the period-2 points, as shown in Fig. 5(b) (v_c = 115.5 mV). In the first return map shown in Fig. 5(c), the period-1 point, with a magnitude of about 0.212, is located on diagonal line while the period-2 points (0.212, 0.230) are symmetrically reflections. By defining period-1 or period-2 points as an event and iteration times between two successive events as IEI, the first return map also exhibits a lattice structure (Fig. 5(d)) and the IEI histogram of this C_{Vm} map also shows exponentially decaying multiple peaks (Fig. 5(e)).



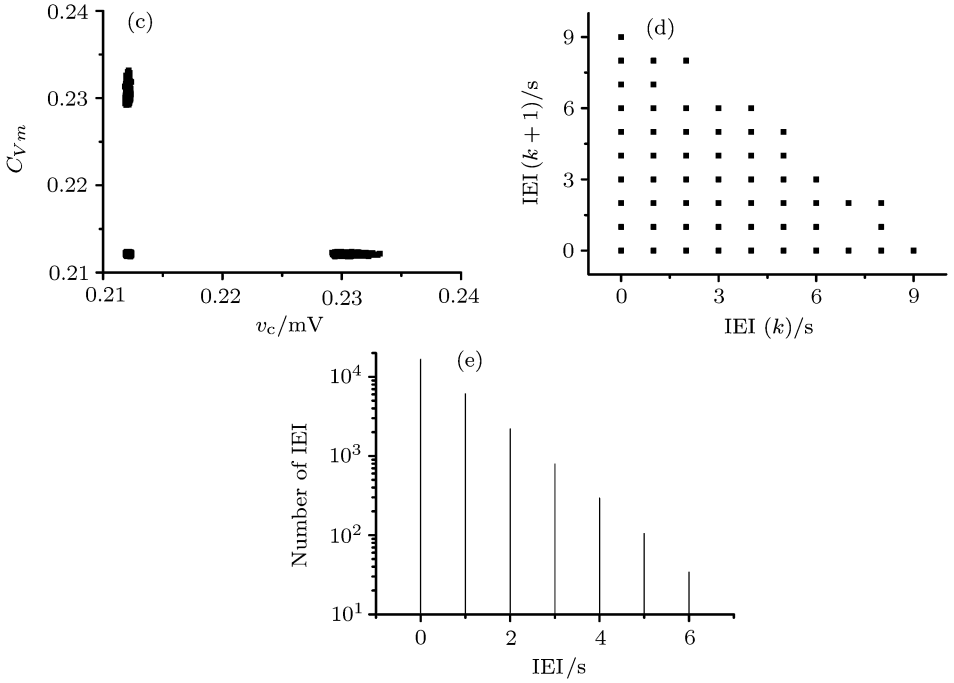


Fig. 5. Characteristics of C_{Vm} map from stochastic Chay model with noise density being 0.0005. (a) The bifurcation diagram of C_{Vm} with respect to v_c. (b) The train of the C_{Vm} series. (c) First return map of C_{Vm} series. (d) The first return map of IEI series with a pair of the period-2 points defined as an event. (e) IEI histogram of (d).

4. Construction of a discontinuous map of C_{Vm}

4.1. A discontinuous map of C_{Vm} for a given value of v_c

For a given value of v_c, the iteration series of a map, $C_{Vm}(k+1) = f(C_{Vm}(k))$ $(k = 1, 2, \ldots, N)$, can be directly obtained from the simulation with deterministic Chay model, starting at various initial values of the continuous variables. As an example with $v_c = 50$ mV, the first return map of C_{Vm} is shown in Fig. 6(a), which exhibits piecewise smooth features with a discontinuous structure and eventually converges to a set of period-3 points labeled with symbol ∇. The mapping shows a clearly discontinuity (or say a gap) at a critical point of $C_{Vm}^{\rm g} = 0.21661$.

Such a first return map can be approximated by a piecewise smooth function with discontinuous characteristics, in which $C_{Vm}(k+1)$=$f(C_{Vm}(k))$ separates one part with a positive slope (Fig. 6(b), left) and the other part is nearly horizontal (Fig. 6(b), right). Replacing C_{Vm} with x, we write this approximation as

$$y = \begin{cases} a_0 x + b_0, & (x < x_{\rm g0}), \\ y^*, & (x \geq x_{\rm g0}), \end{cases} \tag{4}$$

where $a_0 = 0.9936$ (error: 1.0×10^{-4}), $b_0 = 0.00826$ (error: 2.1×10^{-5}) (with a correlation coefficient $R = 0.99998$ between y and $x < x_{\rm g0}$). By linear least square fitting method, we obtain $x_{\rm g0} = 0.21661$ and $y^* = 0.20316$.

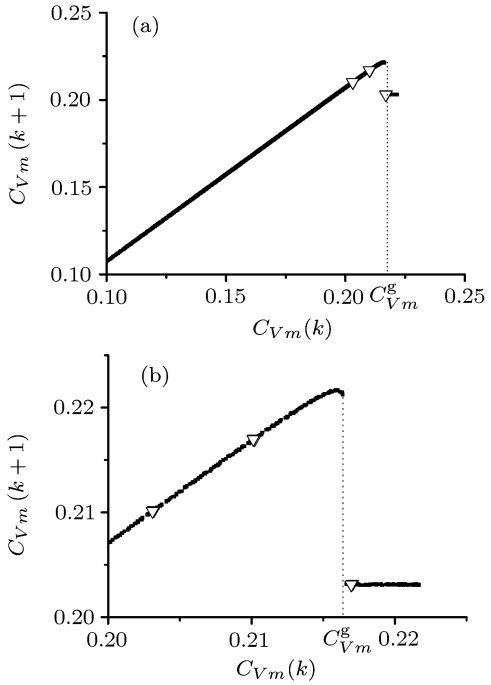


Fig. 6. (a) First return map of C_{Vm} of period-3 bursting acquired from multiple integration realizations with different initial values when $v_c = 50$ mV. (b) Enlargement of (a) to show the discontinuity. Triangle symbols (∇) indicate the period-three points.

4.2. Discontinuous maps with different v_c values

With v_c value chosen as 118 mV, 70 mV, and 50 mV, respectively, the C_{Vm} map obtained from simulation with deterministic Chay model exhibits similar discontinuous structure, as shown in Fig. 7, but

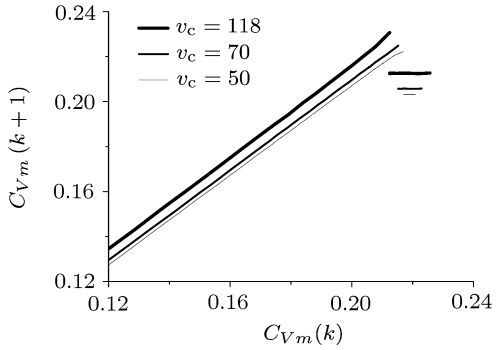


Fig. 7. The first return map of C_{Vm} series simulated in deterministic Chay model with v_c = 118 mV (bold), 70 mV (middle), and 50 mV (thin), respectively.

the position of the two lines shifts downwards with respect to the decrease of v_c. Using linear least square fitting method, we then express the function of C_{Vm} map (C_{Vm} is replaced with x) depending on v_c as:

$$y = f(x, v_c) = \begin{cases} ax + b, & (x < x_{\rm g}), \\ y^*, & (x \geq x_{\rm g}), \end{cases} \tag{5}$$

where a and b are the slope and intercept of the part with a positive slope, respectively. $x_{\rm g}$ stands for values in abscissa for the critical point of discontinuity. y^* stands for values of the horizontal part in ordinate. Parameter v_c is ranging from 32 mV to 150 mV, a, b, $x_{\rm g}$, and y^* are dependent on v_c. a=3.83 × $10^{-4}v_c$ + 0.9749 (with a correlation coefficient R=0.9998). The errors of 3.83 × 10^{-4} and 0.9749 are 7.9 × 10^{-6} and 6.7 × 10^{-4}, respectively. b=5.628 × $10^{-5}v_c$ + 0.0054 (R=0.9997, and errors of 5.628 × 10^{-5} and 0.0054 are 1.49 × 10^{-6} and 1.3 × 10^{-4}, respectively). $x_{\rm g}$=−6.3865 × $10^{-5}v_c$ + 0.2198 (R=0.9997, errors of −6.3865 × 10^{-5} and 0.2198 are 1.7 × 10^{-6} and 1.4 × 10^{-4}, respectively), y^*=1.38 × $10^{-4}v_c$ + 0.1962 (R=0.9996, errors of 1.38 × 10^{-4} and 0.1962 are 3.9 × 10^{-6} and 3.3 × 10^{-4}, respectively).

5. Numeric simulations of the discontinuous map

Taking v_c as a bifurcation parameter, we performed numeric calculation to obtain bifurcation diagrams of the discontinuous map $f(x, v_c)$ with and without introduction of the noise term. The obtained bifurcation diagram from $f(x, v_c)$ without noise (represented by grey line) is shown in comparison with that from deterministic Chay model in Fig. 8(a), it is clearly seen that $f(x, v_c)$ reproduces the period-adding bifurcation scenario simulated in Chay model (represented by black line). Compared with previous studies,[42,49,53] we find that the map with a horizontal right hand part in this paper is a special case. The simulation results of period-adding bifurcation scenario without chaos shown in Figs. 1(a) and Fig. 4(b) in Ref. [53] are similar to Fig. 8(b) in this paper. No chaotic behaviour can be simulated in this discontinuous map with a horizontal right-hand part.[44]

In correspondence with the above experimentation and simulation with the stochastic Chay model, an adding-white noise can also be introduced into the map. The calculated bifurcation diagram using $f(x, v_c)$ with noise (Fig. 8 (b)) with a density D being 0.0001 also exhibits stochastic alternating between period k and period $k+1$ points. An example of such stochastic iteration series between period 1 and period 2 is shown in Figs. 8(c) and 8(d). With a period-1 point or a set of the period-2 points defined as an event, the IEI series also show a lattice structure in the first return map (Fig. 8(e)) and exponentially decaying multiple peaks in IEI histogram (Fig. 8(f)). These calculated results indicate that the constructed discontinuous map precisely reproduces the main features seen in the period-adding bifurcation scenario of ISI in experiment and continuous differential Chay model. Iterations in $f(x, v_c)$ completely reflect dynamic properties of the experimentally observed ISI series, which are dynamic bursting trains employed by neurons to encode information. In the following sections we then performed qualitative analysis with $f(x, v_c)$ to further study mechanisms of the period-adding bifurcation scenario, which underpins transitions of neural bursting patterns.

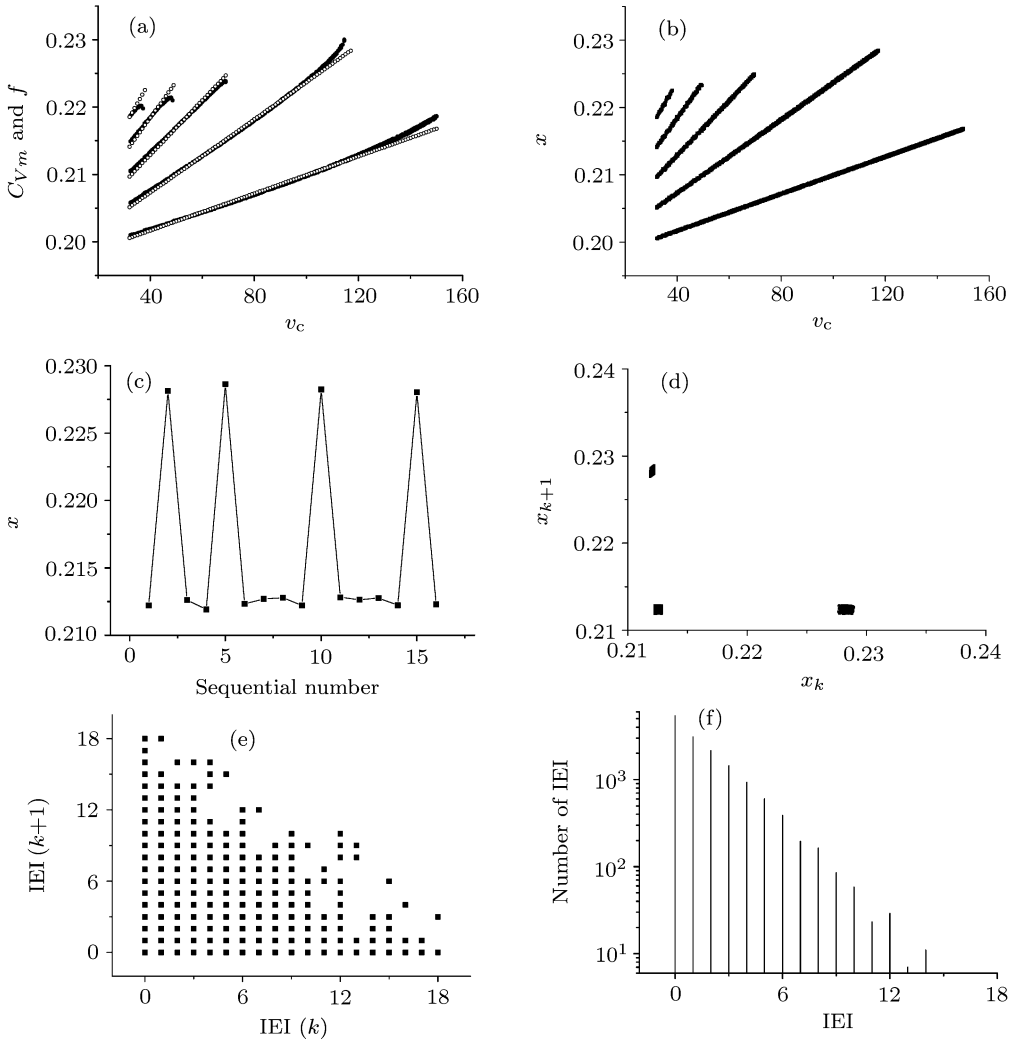


Fig. 8. (a) The bifurcation scenario of C_{Vm} with respect to v_c in the deterministic Chay model (bold black line) and in the map of $f(x, v_c)$ (grey line). (b) The bifurcation scenario of map $f(x, v_c)$ with respect to v_c when noise density was 0.0001. (c)–(f) Behaviours of map $f(x, v_c)$ with noise density 0.0005 when $v_c = 117.8$ mV. (c) The series of the map $f(x, v_c)$. (d) First return map of the series of map $f(x, v_c)$. (e) First return map of IEI series when period-2 points defined as event. (f) The IEI histogram when period-2 points defined as event.

6. The mechanism for the period-adding sequence

In the previous sections we have shown that the dynamics of intracellular calcium concentration could be well approximated by a discontinuous map with piecewise linear characteristics, and the bifurcation diagram of this map exhibits a period-adding cascade without chaos which coincides with the experimental observation. We can therefore understand the mechanism and analytically derive the critical values of the control parameters for transitions between successive periodic orbits involved in the period-adding sequence through a simple analysis to this map. In the next section, based on the codimension-three bifurcation in Ref. [53], we will further analyse the period-adding sequence by applying an established generic concept to this constructed map.

In Fig. 9(a), one may see that there is a discontinuity (or say a gap) at $x_{\rm g}$ which decomposes the phase space of the map into two regions of different characteristics. The left branch is a linear map with its slope and abscissa controlled by parameter v_c. The right branch is a horizontal line positioned at y^* in the vertical axis. It intersects the diagonal at $x = y^*$ when $v_c = 150$ mV. This fixed point is a superstable one because the slope of the right branch is always zero. Thus one observes a stable period-1 orbit. The position of this periodic orbit moves to the left while the boundary (the discontinuous point) between the two regions shifts to right when v_c decreases. The periodic trajectory collides with the discontinuity at boundary $x_{\rm g}$ when the control parameter tends to a critical value $v_c(2)$ (where 2 represents the periodic number of orbits). The collision condition reads

$$y^* = x_{\rm g}. \tag{6}$$

Substituting the control parameter dependence of the mapping function into this equation, we obtained the numeric value of the critical parameter, i.e., $v_c(2) = 117.18$. At this critical point, the period-1 orbit disappears but a period-2 orbit emerges. This is to say that the system undergoes a transition from a period-1 to a period-2 orbit. We can term it as a border-collision bifurcation.[42,51,53]

This collision-induced period-adding transition can be easily understood by considering the discontinuous feature of the current map. Actually, one has to distinguish the left and the right limitations of the map when there is a discontinuity. The right branch of the map intersects the diagonal at the super-stable fixed point $y^* = x_{\rm g}^+$ when $v_c = v_c^+(2)$ (where the superscript "+" implies the right limitation). Hence we have a period-one orbit. In the opposite limitation, i.e., $v_c = v_c^-(2)$, the collision condition changes into $v_c = x_{\rm g}^-$ and the first-order mapping of y^* is no longer determined by the right branch of the mapping function but the left one (see Fig. 9(b)). Therefore, we get a period-2 orbit which is guaranteed by the condition

$$f^2(y^*) = y^*, \tag{7}$$

and correspondingly a transition from the period-1 to the period-2 orbit.

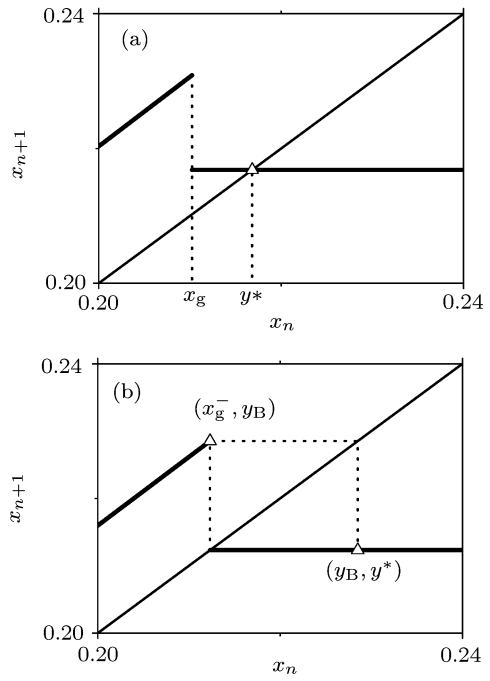


Fig. 9. The first return maps and the corresponding period orbit for different v_c: (a) v_c = 150 mV; (b) $v_c = v_c^-(2)$. Triangle symbol (△) represents stable periodic orbit.

The period-2 trajectories, denoted by y^* and $f(y^*)$, shift to left when v_c decreases. One of them, i.e., $f(y^*)$, collides with the discontinuity when v_c tends to the critical value $v_c(3)$. The value of $v_c(3)$ can be calculated through the collision condition $f(y^*) = x_{\rm g}$. As shown in Fig. 10(a), the trajectory $f(y^*)$ collides with the boundary from the right when v_c tends to $v_c^+(3)$, i.e.,

$$f(y^*) = x_{\rm g}^+. \tag{8}$$

Meanwhile, equation (7) still holds and one can of course observe this period-2 orbit. In the opposite limitation as shown in Fig. 10(b), i.e., $v_c = v_c^-(3)$, the collision condition changes into

$$f(y^*) = x_{\rm g}^-. \tag{9}$$

Consequently, the second-order mapping of y^* is no longer determined by the right branch of the mapping function but the left one. Thus one has the fixed point equation

$$f^3(y^*) = y^*. \tag{10}$$

It implies that there appears a period-3 orbit. Here we show another example of the period-adding cascade due to boundary collision bifurcation, the one from period 2 to period 3.

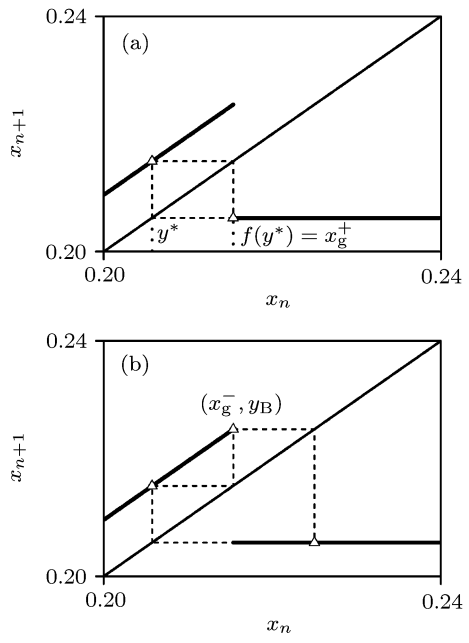


Fig. 10. The first return map and the corresponding periodic orbits when the control parameter is near the critical value $v_c(3)$: (a) for the case of $v_c = v_c^+(2)$; (b) for the case of $v_c = v_c^-(2)$. Triangle symbol (△) represents stable periodic orbit.

We may extend the previous discussion to a generalized transition from a period k to a period $k+1$ orbit when the control parameter goes to the critical value $v_c(k+1)$. The critical value can be calculated by the collision condition

$$f^{k-1}(y^*) = x_{\rm g}. \tag{11}$$

In the right limitation $v_c \to v_c^+(k+1)$, one has

$$f^{k-1}(y^*) = x_{\rm g}^+. \tag{12}$$

Thus we have

$$f^{k}(y^*) = y^*, \tag{13}$$

which shows that there is a period-k motion. While in the left limitation $v_c \to v_c^-(k+1)$, one has

$$f^{k-1}(y^*) = x_{\rm g}^-. \tag{14}$$

The $(k-1)$-order mapping of y^*, i.e., $f^{k-1}(y^*)$ falls in the left branch of the map and thus we get a period-$(k+1)$ orbit, i.e.,

$$f^{k+1}(y^*) = y^*. \tag{15}$$

Therefore one expects a transition from the period k to a period $k+1$ orbit induced by boundary collision bifurcation.

The explicit expression of the fixed point Eq. (11) can be expressed by

$$a^{k-1}y^* + a^{k-2}b + \cdots + ab + b - x_{\rm g} = 0, \tag{16}$$

where $x_{\rm g}$, y^*, a and b depend on the control parameter v_c. The critical values $v_c(k+1)$ can be obtained by solving Eq. (16) for v_c. The numeric results are $v_c(2) = 117.18$ mV, $v_c(3) = 69.42$ mV, $v_c(4) = 49.04$ mV, and $v_c(5) = 37.77$ mV. They are very close to those found in numerical simulations, indicating that the discontinuous map with piecewise linear characteristics constructed in this work indeed captures the essential features for the dynamics of the period-adding cascade.

7. Application of a generic concept to our experimentally observed bifurcation scenario

Previous investigations indicate that the period-adding cascades observed in non-smooth practical systems can be categorized into only a few typical cases.[53] They are pure period increment, period increment with coexistence of attractors, and period-adding scenarios. It has been shown that such bifurcations are generated by repeated occurrence of border collision bifurcation. The bifurcation cascade, namely period adding with stochastic bursting, as we studied in this paper is very likely the pure period increment bifurcation pattern, and thus is a special case of the generic analysis of Ref. [53]. This generic analysis revealed that the complex bifurcation sequences can be understood in terms of only a few codimension-three big bang bifurcations by investigating the normal form of such non-smooth maps. In this section, we applied this concept to our experimentally observed bifurcation sequence in the neural pacemaker system. The normal form can be rewritten as follows:

$$x_{n+1} = \begin{cases} a_1 x_n + u, & (x_n < 0), \\ b_1 x_n + u - L, & (x_n > 0), \end{cases} \tag{17}$$

where a_1 (a in Ref. [53]), b_1 (b in Ref. [53]), u, and L are parameters. What we observed in experiment is very likely the case of negative discontinuity with $L < 0$ (for example $L = 1$ in Ref. [53]) and can be understood by investigating the bifurcation dynamics of the pure period increment. It has been shown in Ref. [53], the pure period increment was studied with $b_1 = 0$, a_1 and u were adjusted along the curve $(u/0.5)^2 + {a_1}^2$=1.

We rewrite the map from continuous Chay model as follows:

$$x_{n+1} = \begin{cases} Ax_n + B, & (x_n < 0), \\ B - C, & (x_n > 0), \end{cases} \tag{18}$$

where

$$A = a, \quad B = (a-1)x_{\rm g}, \quad C = b - y^* + x_{\rm g}, \tag{19}$$

A, B, and C correspond to a_1, u and L in Eq. (17), respectively. v_c is between 150 and 32, so C is positive and the discontinuity is negative.

In Eqs. (18) and (19), parameters are in the range of $1.03235 > A > 0.98716$, $0.02064 > B > 0.0044$, and $0.0139629 > C > 0.02154$, while in Eq. (17), they are in $0 < a_1 < 1$, $0 < u < 0.5$ and $L = 1$. The results of Eq. (17) cannot be directly utilized to interpret the behaviour of Eq. (18), thus we firstly studied the bifurcation structures of Eq. (17) in $a_1 \times u$ plane in which the parameter region is extended to $a_1 > 1$ with $b_1 = 0$, and then applied the analysis to Eq. (18).

We defined $g(x) = a_1 x + u$ and the value of u corresponding to the bifurcation from stable period k to

stable period $k+1$ ($k \geq 1$) as u_{k-k+1}. If $u > L$, there is a stable period-1 point. The $u = L$ is the bifurcation point from period 1 to period 2, labeled as $u_{1-2} = L$. The u_{k-k+1} ($k > 1$) is determined by $g^{k-1}(u-L) = 0$, and u_{k-k+1} can be calculated as follows:

$$u_{k-k+1} = \frac{a_1^{k-1}}{a_1^{k-1} + a_1^{k-2} + \cdots + a_1 + 1} L = \frac{a_1^{k-1}}{\sum_{i=0}^{k-1} a_1^i} L \quad (k > 1). \tag{20}$$

Considering $u_{1-2} = L$, when $0 < a_1 < 1$, we have

$$u_{k-k+1} = \frac{a_1^{k-1}}{\sum_{i=0}^{k-1} a_1^i} L \quad (k > 1), \tag{21}$$

the value of u_{k-k+1} approaches 0 when k approaches infinity. It can be described as

$$\lim_{k\to\infty} u_{k-k+1} = u_\infty = 0 \quad (0 < a_1 < 1), \tag{22}$$

u_∞ is the value of u when the period number of the orbit approaches infinity.

When $a_1 > 1$, if $g(u-L) < u - L$, the next iterative point is more negative than $u - L$, and an iterative procedure in which the next iterative point is even more negative is formed. There appears no stable periodic orbit. If $g(u-L)$ is changed from a value bigger than $u - L$ to what smaller than $u - L$ when u is decreased, the existing periodic orbit disappears. The $g(u-L) = u - L$ is a critical value across which stable period orbits appear or disappear, which corresponds to the equation

$$u = (1 - 1/a_1)L. \tag{23}$$

In fact,

$$\lim_{k\to\infty} u_{k-k+1} = (1 - 1/a_1)L \quad (a_1 > 1), \tag{24}$$

then $u = (1-1/a_1)L$ is the limit of the stable periodic orbit whose periodic number approaches infinity, i.e. u_∞.

Therefore, the surfaces u_{k-k+1} (k=1, 2, 3,...,∞) are composed of the codimension-one bifurcation point in $a_1 \times u \times L$ parameter region. ($a_1 = 0$, $u = 0$) is a codimension-two border collision bifurcation point. When one, two, or three parameters of a_1, u and L are changed across the surface u_{k-k+1} via a point far from the higher codimension bifurcation point, codimension-one border collision bifurcation is generated.

We illustrated the bifurcation structures in $a_1 \times u$ plane with L fixed at various values to show the intersection lines between surface u_{k-k+1} and plane L. The bifurcation structures in plane ($0 < a_1 < 1.5$) with L=1 are shown in Figs. 11(a) and 11(b). From top to bottom, 26 lines corresponding to u_{k-k+1} (k=1, 2, ..., 26) and u_∞ ($a_1 > 1$) are used to show the increment of period when the parameter is adjusted across the lines. If L is changed to a different value, the changes of u_{k-k+1} is proportional to L (not shown here).

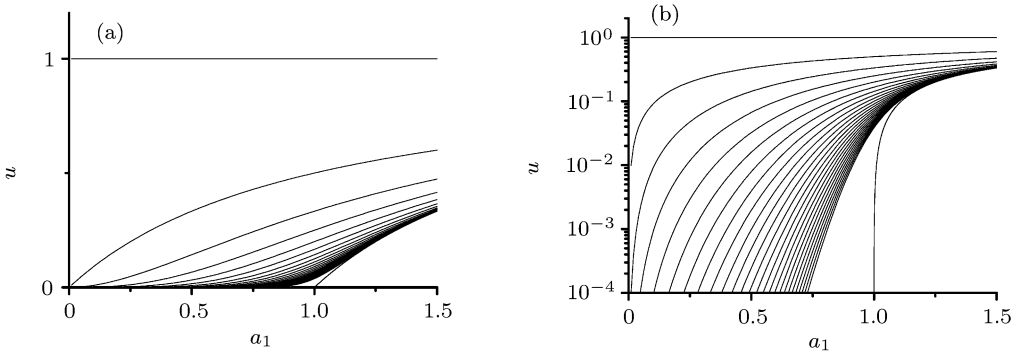


Fig. 11. Two-parameter bifurcation diagrams in $a_1 \times u$ plane when $L = -1$ and $b_1 = 0$, point (a_1=0, u=0) is a big bang bifurcation point: (a) linear scale; (b) logarithm scale. The behaviour in the area corresponding to $0 < a_1 < 1$ and $0 < u < 0.5$ was shown in Fig. 4(a) in Ref. [53].

In what follows we applied the analysis to Eq. (18). Bifurcation structures of Eq. (18) in the parameter region $A \times B \times C$ are calculated when A, B and C are changed independently. The border collision bifurcation surfaces B_{k-k+1} are as follows:

$$B_{k-k+1} = \frac{A^{k-1}}{A^{k-1} + A^{k-2} + \cdots + A + 1} L = \frac{A^{k-1}}{\sum_{i=0}^{k-1} A^i} L \quad (k = 1, 2, \ldots, \infty), \tag{25}$$

where $B_\infty = 0$ $(A < 1)$, $B_\infty = (1 - 1/A)C$ $(A > 1)$.

The B_{k-k+1} is similar to u_{k-k+1} in Eq. (17). The two-parameter bifurcation structures of Eq. (18) in $A \times B$ plane with C fixed at 5 different values are shown in Figs. 12(a)–12(e), respectively. Equation (19) yields that the covariation of A, B and C is restricted by the changes of parameter v_c, which is of biological importance and was adjusted in our experiments. This guarantees that A, B, and C vary together to across the surfaces B_{k-k+1}. As shown in Figs. 12(a)–12(e), when the values of C corresponding to critical values of v_c =150, 100, 56, 43 and 32 are calculated according to Eq. (19), respectively, the corresponding values of A and B are located at the bifurcation parameter region from period 1, to 2, to 3, to 4, and to 5, respectively. Such results clearly show that the pure period increment in Eq. (18) driven by adjustment of v_c is realized by the joint variation of A, B, and C to across the border collision bifurcation surface B_{k-k+1}. This bifurcation dynamics is the same as what occurs in Eq. (17) in the case of a negative discontinuity.

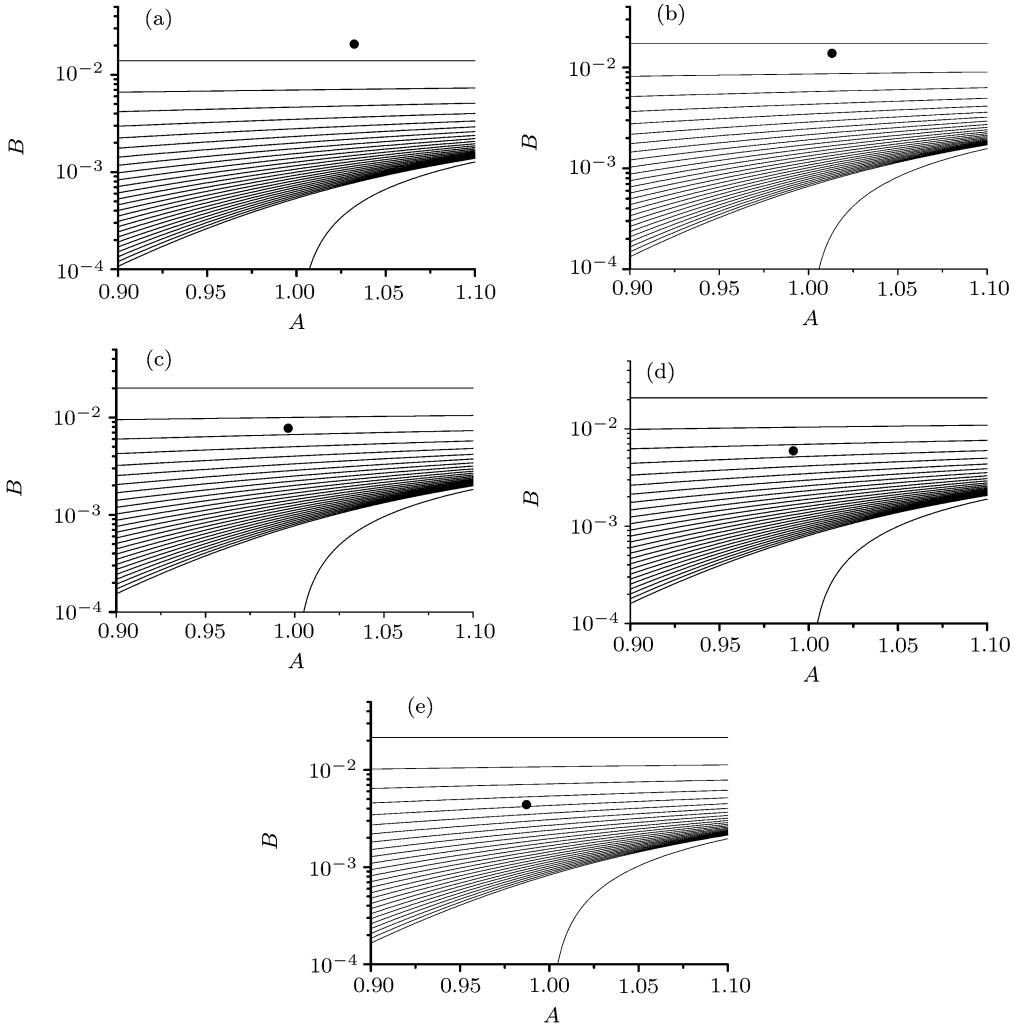


Fig. 12. Two-parameter bifurcation diagrams in $A \times B$ plane near $A = 1$ at different C values. (a) $C = 0.013963$; (b) $C = 0.017259$; (c) $C = 0.020058$; (d) $C = 0.020866$; (e) $C = 0.021540$. The black cycle in each figure corresponds to the parameter of A, B and C determined by $v_c = 150$ mV, 100 mV, 56 mV, 43 mV and 32 mV. From (a) to (e), the behaviours are period 1, 2, 3, 4 and 5 respectively.

8. Discussion and conclusion

In the present paper, we analysed the border-collision bifurcation by a simple discontinuous map that captures essential features of the period-adding bifurcation scenarios observed in both experiment and simulations with the differential Chay model. Our particularly designed experiment shows typical bifurcations with stochastic bursting patterns induced by fluctuations in real neuronal systems. Adding a white noise term into the Chay

model, we find that the constructed discontinuous map reproduces and explains the stochastic bursting patterns. Employing this simple discontinuous map controlled by a slow variable, we interpret not only the structure of the first return map formed by ISI series of the periodic bursting but also the mechanism for the transition from period k to period $k+1$ bursting. The effect of noise on behaviours near the bifurcation point,[35,55,56] such as spiking or bursting near the parameter region from spiking to bursting, was studied in a previous study.[35] Type I bursting and type II bursting were induced when noise was introduced into the first and third equations of the theoretical models, respectively. Correspondingly, the perturbation in the fast subsystem and in slow subsystem played a dominant role, respectively. The conclusion is also helpful for further understanding of the stochastic bursting pattern in this paper. Furthermore we explain the period-adding bifurcation cascade in terms of the border-collision bifurcation associated with discontinuous property of this map. This slow variable has been demonstrated to be the control mechanism initiating and terminating the spike trains of the fast subsystem and thus determining the period number of the bursting. Moreover, deduction from the constructed discontinuous map precisely predicts the parameter values corresponding to each bifurcation in the period-adding scenario, providing a simple and clear mathematical formula for neuronal firing pattern transitions. Simpler formulas like the one that we provided in this paper might be of important practical use in modeling collective behaviours of large neural populations, for example, synchronization in bursting timing seen in a variety of neural circuits ranging from thalamus to cerebral cortex.

A previously established concept revealed the codimension-three bifurcation dynamics underlying the period increment sequence.[53] The neuronal period adding cascade with stochastic bursting, as we studied in this paper, is the pure period increment bifurcation pattern. The mechanism of this pure period increment is given as a special case of the generic concept. Thus, we applied this concept to our constructed map. Based on the available codimension-three big bang bifurcation points, we identified the codimension-two and codimension-one border collision bifurcation. It is clearly seen that the period increment is generated by repeated occurrence of border collision bifurcation. Similar analysis can be applied to other bifurcations, which have been systematically studied in a number of works.[18,20,29]

In recent years, non-smooth or discontinuous maps have been successfully applied to studies of period doubling and period-adding bifurcation cascades observed in various nonlinear systems with non-smooth or discontinuous characteristics, including mechanical systems involving friction, electrical circuits containing diodes, transistors, earthquake engineering.[34−50] In biological systems, pulsatile behaviours such as spiking and bursting in nerve or cardiac cells exhibit obvious discontinuous characteristics.[9,10,12,13,31,32,36] The voltage spikes increase first and then decrease sharply within less than 10 msec. The sharp changes in voltage manifest characteristics similar to those of non-smooth systems and regarded as quasi-discontinuous characteristics in a number of previous literatures.[12,13] Neuronal firing patterns also manifest discontinuities. Neuronal systems generating complex firing patterns are usually composed of a fast subsystem and a slow subsystem.[2,14] The fast subsystem generates sharp spikes by sodium and potassium ionic currents while the slow subsystem modulates the bursting pattern of the spikes by a slow variable. Thus, maps of this slow variable in Poincaré section of spike maximum values reflects the effects of this slow control variable and captures the essential features of transition between bursting patterns. For example, the discontinuous characteristics exhibited in the first return map of the slow variable in Hindmarsh–Rose model can be used to interpret the intermittency and period doubling to chaos.[12,13] In accordance with previous studies, the discontinuous map of C_{Vm} in the present study reproduces the dynamics of a series of bursting patterns, and furthermore, reveals the mechanism of bifurcations in period-adding cascade. Therefore, the results of the present study provide an example of usage of discontinuous maps to interpret neuronal bifurcation cascade.

In fact, the discontinuous phenomena have been observed in activities at various levels of the nervous system,[9,10,12,13,31,32,36] ranging from firing patterns in single nerve cells to electro-encephalogram of large neuronal populations. Such neural activities exhibit typical discontinuous characteristics and provide ideal subjects for nonlinear dynamical researches. For example, except the period-adding bifurcation scenario studied in this paper, discontinuities in period doubling routing to chaos[18,20] and the non-smooth features of the chaotic patterns[18,20,22−24,28] seen in neuronal bursting are also remained to be elucidated.

References

[1] Rachwalska M and Kawczyński A L 2001 *J. Phys. Chem.* A **105** 7885
[2] Izhikevich E M 2000 *Int. J. Bifur. Chaos* **10** 1171
[3] Yang M H, An S C, Gu H G, Liu Z Q and Ren W 2006 *NeuroReport* **17** 995
[4] Braun H A, Wissing H, Schäfer K and Hirsch M C 1994 *Nature* **367** 270
[5] Chay T R 1985 *Physica* D **16** 233
[6] Fan Y S and Chay T R 1994 *Biol. Cybern.* **171** 417
[7] Chay T R and Fan Y S 1995 *Int. J. Bifur. Chaos* **5** 595
[8] Hindmarsh J L and Rose R M 1984 *Proc. R. Soc. London* Ser. B **221** 87
[9] Holden A V and Fan Y S 1992 *Chaos, Solitons and Fractals* **2** 583
[10] Fan Y S and Holden A V 1993 *Chaos, Solitons and Fractals* **3** 439
[11] Terman D 1992 *J. Nonlinear Sci.* **2** 135
[12] Wu S G and He D R 2001 *Commun. Theor. Phys.* **35** 275
[13] Wu S G and He D R 2001 *J. Phys. Soc. Jpn.* **70** 69
[14] Rinzel J and Lee Y S 1987 *J. Math. Biol.* **25** 653
[15] Del Negro C A, Hsiao C F, Chandler S H and Garfinkel A 1998 *Biophys. J.* **75** 174
[16] Shilnikov A and Cymbalyuk G 2005 *Phys. Rev. Lett.* **94** 048101
[17] Channell P, Cymbalyuk G and Shilnikov A 2007 *Phys. Rev. Lett.* **98** 134101
[18] Ren W, Hu S J, Zhang B J, Wang F Z, Gong Y F and Xu J X 1997 *Int. J. Bifur. Chaos* **7** 1867
[19] Xu J X, Gong Y F and Ren W 1997 *Physica* D **100** 212
[20] Li L, Gu H G, Yang M H, Liu Z Q and Ren W 2004 *Int. J. Bifur. Chaos* **14** 1813
[21] Gu H G, Yang M H, Li L, Liu Z Q and Ren W 2003 *Phys. Lett.* A **319** 89
[22] Gu H G, Yang M H, Li L, Ren W and Lu Q S 2007 *Dyn. Contin. Discr. Impul. Syst. (Series B: Applications & Algorithms)* **14** 6
[23] Yang M H, Gu H G, Li L, Liu Z Q and Ren W 2003 *NeuroReport* **14** 2153
[24] Ren W, Gu H G, Jian Z, Lu Q S and Yang M H 2001 *NeuroReport* **12** 2121
[25] Gu H G, Ren W, Lu Q S, Wu S G, Yang M H and Chen W J 2001 *Phys. Lett.* A **285** 63
[26] Yang M H, Li L, Liu Z Q, Liu H J, Xu Y L, Gu H G and Ren W 2009 *Int. J. Bifur. Chaos* **19** 453
[27] Wu X B, Mo J, Yang M H, Zheng Q H, Gu H G and Ren W 2008 *Chin. Phys. Lett.* **25** 2799
[28] Zheng Q H, Liu Z Q, Yang M H, Wu X B, Gu H G and Ren W 2009 *Phys. Lett.* A **373** 540
[29] Yang Z Q, Lu Q S and Li L 2006 *Chaos, Solitons and Fractals* **27** 689
[30] Duan L X, Lu Q S and Wang Q Y 2008 *Neurocomputing* **72** 341
[31] Coombes S and Osbaldestin A H 2000 *Phys. Rev.* E **62** 4057
[32] Medvedev G S 2005 *Physica* D **202** 37
[33] Douglass J K, Wilkens L, Pantazelou E and Moss F 1993 *Nature* **365** 337
[34] Medvedev G S 2006 *Phys. Rev. Lett.* **97** 048102
[35] Hitczenko P and Medvedev G S 2009 *SIAM J. Appl. Math.* **69** 1359
[36] Bressloff P C and Stark J 1990 *Phys. Lett.* A **150** 187
[37] Christiansen B, He D R, Habip S, Bauer M and Krueger U 1992 *Phys. Rev.* A **45** 8450
[38] Nusse H E and Yorke J A 1992 *Physica* D **57** 39
[39] Nusse H E, Ott E and Yorke J A 1994 *Phys. Rev.* E **49** 1073
[40] Nusse H E and Yorke J A 1995 *Int. J. Bifur. Chaos* **5** 189
[41] Qu S X, Wu S G and He D R 1997 *Phys. Lett.* A **231** 152
[42] Qu S X, Wu S G and He D R 1998 *Phys. Rev.* E **57** 402
[43] Bernardo M Di, Feigin M I, Hogan S J and Homer M E 1999 *Chaos, Solitons and Fractals* **10** 1881
[44] Jain P and Banerjee S 2003 *Int. J. Bifur. Chaos* **13** 3341
[45] Sharkovsky A N and Chua L Q 1993 *IEEE Trans. Circuit Sys.* I **40** 722
[46] Halse C, Homer M and Bernardo M Di 2003 *Chaos, Solitons and Fractals* **18** 953
[47] Belykh V N and Belykh I V 2000 *Eur. Phys. J.* E **3** 205
[48] Kollár L E, Stépán G and Turi J 2004 *Int. J. Bifur. Chaos* **14** 2341
[49] Avrutin V and Schanz M 2004 *Phys. Rev.* E **70** 026222
[50] Avrutin V and Schanz M 2005 *Int. J. Bifur. Chaos* **15** 1267
[51] Hogan S J, Higham L and Griffin T C L 2007 *Proc. R. Soc.* A **463** 49
[52] Dutta P S, Routroy B, Banerjee S and Alam S S 2008 *Nonlinear. Dyn.* **53** 369
[53] Avrutin V, Schanz M and Banerjee S 2007 *Phys. Rev.* E **75** 066205
[54] Mannella R and Palleschi V 1989 *Phys. Rev.* A **40** 3381
[55] Ni F, Xu W, Fang T and Yue X L 2010 *Chin. Phys.* B **19** 010510
[56] Feng J Q, Xu W and Niu Y J 2010 *Acta Phys. Sin.* **59** 157 (in Chinese)